Infrared vibrations in $LaSrGaO_4$ and $LaSrAlO_4$

J. Humlíček,* R. Henn, and M. Cardona
Max-Planck-Institut für Festkörperforschung, Heisenbergstrasse 1, D-70569 Stuttgart, Germany
(Received 9 November 1999)

We have studied the *c*-axis and the in-plane infrared response of the anisotropic crystals of $LaSrGaO_4$ and $LaSrAlO_4$. We identify both transverse and longitudinal phonons. The lattice bands show pronounced features of mode coupling, which we attribute to the random distribution of La and Sr atoms in the lattice. We present a scheme to identify and quantify the coupling that induces the asymmetric line shapes. We use the results to discuss infrared-active vibrations of other compounds, including La_2CuO_4.

I. INTRODUCTION

The insulating crystals of lanthanum strontium gallate, $LaSrGaO_4$ (LSGO) and aluminate, $LaSrAlO_4$ (LSAO) are interesting materials from several points of view. They have the same tetragonal structure as the simplest ''single-layer'' high-T_c superconductor $La_{2-x}Sr_xCuO_4$, the so-called *T* structure.[1] Their vibrational properties are closely related to those of the high-temperature tetragonal phase of the insulating parent compound of this superconductor, La_2CuO_4, similarly as for the isostructural compound La_2NiO_4.[2] Since there are still ambiguities in assigning zone-center phonons in $La_{2-x}Sr_xCuO_4$,[3] the results for LSGO and LSAO allow a better understanding of the topic. Due to a fairly good lattice matching to a variety of superconducting cuprates, and low dielectric losses in far-infrared and microwave ranges, LSAO and LSGO are attractive as substrates for growing epitaxial films.[4,5] Recently, results of Raman and infrared studies were reported for LSAO (Ref. 6) and infrared reflectance studies were performed for both LSGO and LSAO.[7] In both compounds the Sr^{2+} and La^{3+} ions are distributed randomly over the sites of C_{4v} symmetry in the lattice of the K_2NiF_4 structure[8] which is shown schematically in Fig. 1. This situation should favor possible coupling of vibrational eigenmodes.

In the present paper, we use the technique of ellipsometry to investigate the infrared vibrations of LSGO and LSAO. We aim mainly at the extraction of transverse and longitudinal phonon parameters, and at the identification of mode coupling. We also discuss the zone-center phonon frequencies of several *T*-structure compounds obtained from infrared and neutron-scattering studies.

II. EXPERIMENT AND DATA EVALUATION

High-purity LSGO and LSAO single crystals were grown by the Czochralski method, as described in detail in Refs. 9 and 10. The crystals were cut in rectangular pieces of about $7\times7\times1$ mm^3 with the *c* axis either in the sample surface or perpendicular to it. After polishing large faces to optical quality, the samples were found to be transparent in the visible, though lightly yellow colored. A very weak visible absorption responsible for the color starts at the photon energy of about 2.5 eV;[11] it is known to be due to point oxygen defects (vacancies and interstitials).[10] We have also investigated one sample of $LaSrAl_{0.75}Ga_{0.25}O_4$ alloy with the *c* axis perpendicular to the sample surface. Its smaller dimensions ($5\times5\times0.5$ mm^3) did not allow us to measure its optical response for electric fields along the *c* axis. The lattice parameters of the three materials are listed in Table I.

The optical measurements were performed with two home-built ellipsometers, one attached to a Bruker 113v,[12] the other to a Bruker IFS55[13] Fourier-transform spectrometer, covering far- (50–700 cm^{-1}) and mid-infrared ranges (400–2000 cm^{-1}), respectively. In the far-infrared setup, the samples were mounted in a continuous helium flow cryostat in which the temperature could be varied between 10 and 300 K. The low-temperature data display sharper phonon bands which are helpful in identifying weaker modes. The angle of incidence was either 75 or 80°. The mid-infrared data were taken at room temperature, with the angle of incidence ranging from 30 to 80°.

The ellipsometric measurements have been performed for all three high-symmetry orientations of the optical axis with

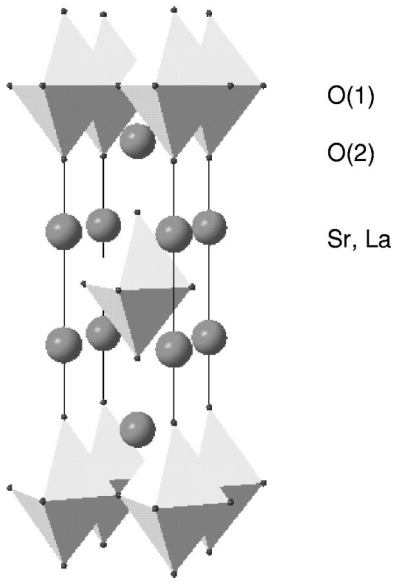

FIG. 1. Polyhedral representation of the structure of $LaSrGaO_4$ and $LaSrAlO_4$ crystals. Ga or Al are located at the centers of oxygen octahedra. Sr and La are shown as the large spheres; they are distributed randomly in the planes close to those of apex oxygen O(2).

TABLE I. Lattice constants (a, b, and c) and volume of the unit cell (V) of $LaSrGaO_4$, $LaSrAlO_4$, and their alloy.

	$a=b$ (nm)	c (nm)	V(nm^3)	Ref.
$LaSrGaO_4$	0.3843	1.2681	0.18728	25
$LaSrAlO_4$	0.37564	1.26357	0.17829	8
$LaSrGa_{0.25}Al_{0.75}O_4$	0.3772	1.266	0.18013	26

respect to the plane of incidence of the light. We denote them by using for the crystallographic axes the symbols x_1, x_2, and x_3, ordered in a single symbol (x_1x_2-x_3). Here, the first letter in brackets means the direction of intersection of the sample surface with the plane of incidence, the second the direction within the sample surface perpendicular to the plane of incidence, and the third (separated by the dash) the direction perpendicular to the sample surface. Thus, with $x_1=x_2=a$, $x_3=c$ for our uniaxial crystals, the measured orientations of the c axis are: (i) perpendicular to the surface, (aa-c); (ii) in the surface and in the plane of incidence, (ca-a); (iii) in the surface and perpendicular to the plane of incidence, (ac-a). With only a single angle of incidence being measured for each orientation, the data consist of three pairs of real values of the ellipsometric angles (ψ and Δ) for any wave number. The raw ellipsometric data are conveniently represented by $\tan\psi$ and $\cos\Delta$ in our measurements without a retarder:

$$\tan\psi(\cos\Delta + i\sin\Delta) = r_p/r_s, \tag{1}$$

where r_p and r_s amplitude reflectivities for p- and s-polarized light. For the high-symmetry orientations, r_p and r_s are related to principal components of the dielectric tensor of the sample by simple Fresnel formulas.[14] We have used at least three measured pairs of ($\tan\psi$,$\cos\Delta$) to determine the four unknown parameters of our samples, i.e., the pair of complex dielectric functions ε_a and ε_c, of the ordinary and extraordinary response, respectively. The problem becomes even more overdetermined for the measurements at multiple angles of incidence which we have used to check the consistency of the results. A nonlinear fitting procedure[15] has been employed for the point-by-point extraction of the dielectric functions over the measured spectral range. The results obtained at different spectral points are independent of each other, in spite of the fact that we use the output at the former spectral points as the initial estimate for the next. In fact, the fitting either converges to an acceptable solution, or it branches out to an unphysical solution which is easily recognized and discarded.[15] In order to decrease the probability of slipping into unphysical solutions in ranges of very sharp spectral structures, we have used an extrapolation scheme based on several already computed values. Either the complex dielectric function ε or its inverse $1/\varepsilon$, whichever was smaller and smoother, were extrapolated. Let us reemphasize the main advantage of the ellipsometric technique for the present study: the spectral dependence of the complex response functions is obtained on the point-by-point basis throughout the covered spectral range.

We have also measured the mid-infrared reflectivity of the samples that have the optical axis in the surface. Using s-polarized light (i.e., the electric field of the light wave perpendicular to the plane of incidence), the optical axis was oriented either parallel or perpendicular to the plane of incidence. At these orientations, the probed response is that of the extraordinary (c-axis) or ordinary (in-plane) beams, respectively, influenced by the oblique incidence of the light wave. The angles of incidence ranged from 10° (''near-normal incidence'') to 60°. The reference signals were taken from a gold mirror and a thick slice of undoped silicon with a rough back side. We assumed 100% reflectivity for gold. The s- and p-polarized reflectivities computed from its refractive index[16] have been employed in the case of the silicon reference. We used a pair of wire-grid polarizers aligned in tandem to avoid polarization leakage. The reflectance data were generally in very good agreement with the richer information obtained from the ellipsometric measurements.

III. RESULTS AND DISCUSSION

We show in Fig. 2 the ellipsometric data of LSGO obtained at low temperature for the high-symmetry orientations. The spectra display characteristic patterns for the high-reflectivity bands (''reststrahlen bands'') between the strongest TO and LO modes, with pronounced features due to additional weaker TO-LO pairs. We also show in Fig. 2 the mode frequencies obtained from the analysis given below. The situation is fairly simple for photon energies below about 500 cm^{-1} where the magnitudes of both c-axis and in-plane dielectric functions are large. In this case, the data are similar to the results that would be obtained for an isotropic material having the response of the actually measured sample along the intersection of its surface and plane of incidence,[17] i.e., that of the c axis for (ca-a), and in plane for the two remaining orientations. This approximate solution can be understood as follows: (i) the light propagates nearly normally to the surface inside the sample in spite of the oblique incidence, (ii) the ratio r_p/r_s is insensitive to the response perpendicular to the plane of incidence, i.e., to the s-polarized reflectivity, as long as $r_s \approx \pm 1$; this condition is fulfilled for highly polarizable materials at large angles of incidence. Note that the (aa-c) and (ac-a) spectra in Fig. 2 differ for lower wave numbers mainly due to the different angles of incidence, 75 and 80°, respectively.

However, this simple situation changes for higher wave numbers (above ~500 cm^{-1} for LSGO), where the magnitude of ε becomes small. Since the corresponding magnitudes of $1/\varepsilon$ are large, this is the range of the strongly polar LO modes. The ellipsometric ratio r_p/r_s is then dependent on both, the in-plane optical constants and those along the c axis. In particular, the magnitude of r_s can approach zero in a wave-number range where the refractive index for s-polarized light approaches unity (i.e., the optical contrast between the sample and ambient vanishes). If, at the same time, the refractive index in the other direction differs from unity, $\tan\psi = |r_p/r_s|$ becomes large. We can therefore observe spikes or bands in ψ with $\tan\psi$ well above 1, such as shown in Fig. 2, which is impossible for an isotropic sample. The numerical inversion of the ellipsometric equations still provides the correct response functions. However, the use of fairly low angles of incidence (well below 45°) is required in the range of strong LO vibrations in order to optimize sensitivity.[18]

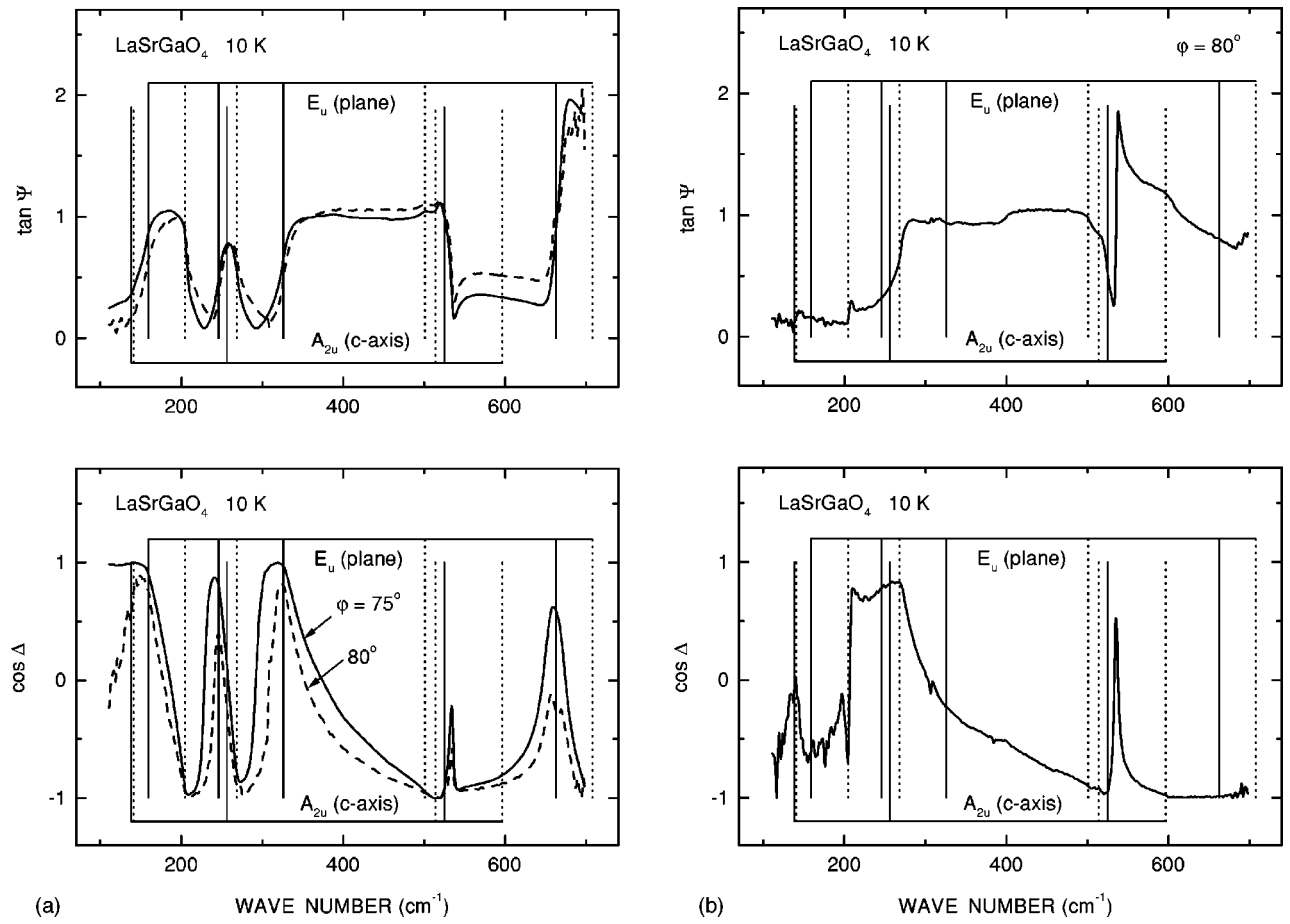

FIG. 2. Low-temperature ellipsometric spectra of $LaSrGaO_4$ measured with an angle of incidence of either 75 or 80 ° for the three high-symmetry orientations. Part (a): $(aa\text{-}c)$, 75 °, solid lines; $(ac\text{-}a)$, 80 °, dashed lines. Part (b): $(ca\text{-}a)$, 80 °. Long vertical lines show the positions of TO (solid) and LO (dots) modes for the electric field parallel (A_{2u}) and perpendicular (E_u) to the c axis. Long horizontal lines just span the range between the lowest TO and highest LO vibrations for the in-plane and c axis polarizations.

A. Infrared spectra of $LaSrGaO_4$ and $LaSrAlO_4$

We have displayed in Figs. 3–6 the room-temperature dielectric functions and their inverses, obtained from our ellipsometric data. Three and four bands can easily be identified for the polarization along the c axis (vibrations of A_{2u} symmetry) and perpendicular to it (E_u), respectively, as required by the symmetry of the $I4/mmm$ structure.[19] Slight signatures of extra structures are seen in the c-axis response of Figs. 3 and 4 at $\sim$500 cm^{-1} in LSGO and at $\sim$580 cm^{-1} in LSAO. They are very probably spurious, resulting from a cross talk of the in-plane direction with sharp and strong LO modes around these frequencies. Related spectral structures were apparently also observed in the reflectivity studies of Ref. 7, although they were interpreted as genuine phonon modes. We show in Fig. 7 a comparison of our measured reflectance at 10 ° off normal incidence, using s-polarized light in $(ac\text{-}a)$ configuration, with the data produced after parametrization of Ref. 7 using Fresnel equations. Both spectra agree quite well in the position of the minimum near 560 cm^{-1} which is related to the TO-LO mode pair at 568 and 555 cm^{-1}, polarized along the c axis. However, the spectral structure at 580 cm^{-1} is much weaker in our directly measured reflectivity. In our opinion, this is due to the strong in-plane LO mode (see Fig. 6) because of imperfect alignment and/or sample miscut, and/or polarization leakage. We were not able to remove it completely from the ellipsometric and reflectance spectra in spite of the attention paid to the possible nonideality of samples and measurement procedures. Simulated spectra confirm the high sensitivity of observed c-axis line shapes to the misalignment in the presence of sharp and strong in-plane LO modes; on the other hand, this influence is restricted to specific narrow spectral ranges. We have therefore omitted the spectral intervals of spurious structures from the analysis that follows.

Some of the observed bands are fairly broad, such as the strongest A_{2u} TO and LO modes of LSGO at 254 and 597 cm^{-1}. In general, the spectral features of LSGO are broader than the corresponding bands of LSAO which occur at higher frequencies. Another remarkable feature is a pronounced asymmetry of several bands. It can be seen, e.g., as the steeper rise and flatter fall of the imaginary part of ε for the 568 cm^{-1} band of LSAO in Fig. 3, when going from smaller to higher wave numbers. This is consistent with the observed sharper maximum and flatter minimum of the corresponding structure in the real part, as required by the Kramers-Kronig relations. The opposite type of asymmetry occurs for the 326 and 445 cm^{-1} E_u modes of LSGO and LSAO, respectively, as seen in Fig. 5. This behavior suggests pronounced mode coupling, expected because of the random occupation of lattice sites by Sr and La ions, which leads to

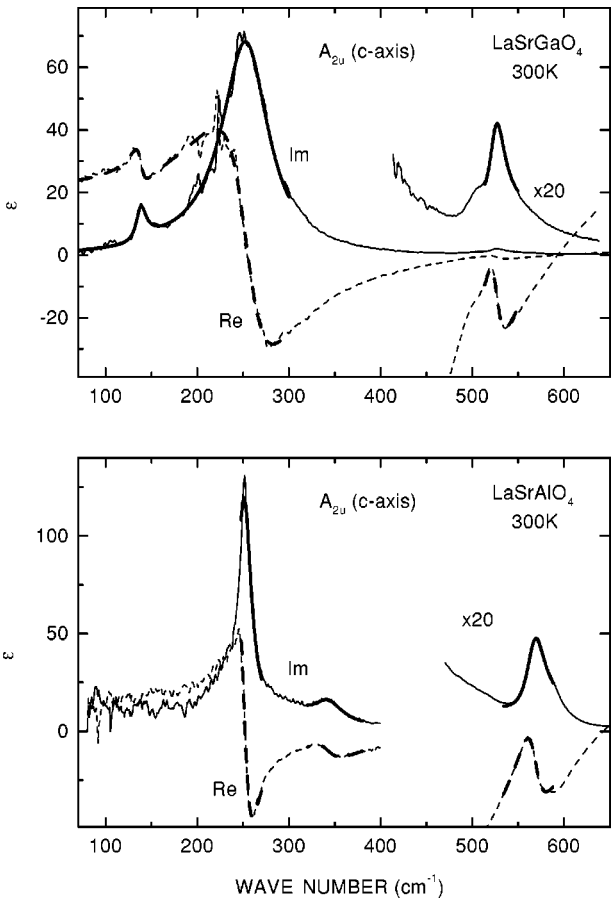

FIG. 3. The real (dashed lines) and imaginary (solid lines) parts of the c component of the dielectric tensor of $LaSrGaO_4$ (upper panel) and $LaSrAlO_4$ (lower panel) crystals. The thick lines represent best fits with modified Lorentzians (accounting for mode coupling) in restricted spectral ranges.

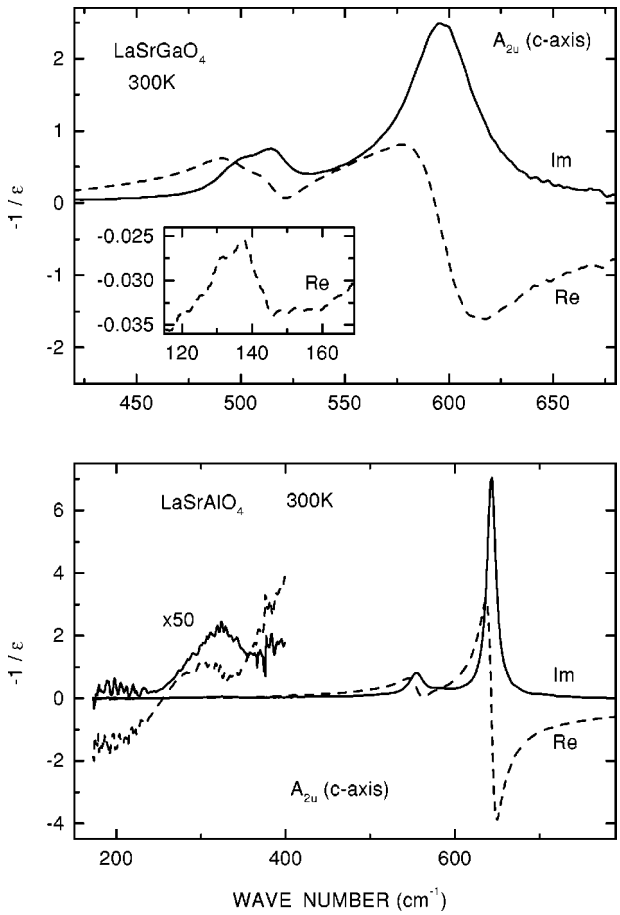

FIG. 4. The real (dashed lines) and imaginary (solid lines) parts of the c component of the negative inverse of the dielectric tensor of $LaSrGaO_4$ (upper panel) and $LaSrAlO_4$ (lower panel) crystals. The weak structure corresponding to the 140-cm^{-1} LO mode of $LaSrGaO_4$ is shown with expanded scales in the inset.

the loss of ideal crystal symmetry. The resulting nonconservation of wave vector **k** contributes essentially one-phonon channels for the decay of excited modes in addition to the multiphonon processes.

A classical phenomenological model of two coupled oscillators has been used by Barker and Hopfield to explain asymmetry and interaction damping of optical phonons observed in several perovskite materials.[20] Our case is more complex due to the larger number of infrared-active vibrational modes. We proceed to introduce the phenomenological scheme used here, and discuss its link with the model of classical coupled oscillators.

B. Response of interacting modes

In agreement with Ref. 20 we define a ''K-mode'' dielectric function ε as a response function having K pairs of simple poles. They are placed in the lower complex half plane of frequencies ω in positions symmetric with respect to the imaginary axis. The electric displacement $D=\varepsilon E$ due to the driving electric field with a harmonic temporal dependence $E=E_0\exp(-i\omega t)$ is proportional to its amplitude E_0. The function $\varepsilon(\omega)$ having K pairs of poles can be written in the following form:

$$\varepsilon(\omega)=\varepsilon_1(\omega)+i\varepsilon_2(\omega)=\varepsilon_\infty+\sum_{j=1}^{K} S_j\frac{\Omega_j^2-i\omega\sigma_j}{\Omega_j^2-\omega^2-i\omega\Gamma_j}. \tag{2}$$

With all of its parameters being real, Eq. (2) satisfies the requirement of obtaining its complex conjugate upon changing the sign of ω. The background term ε_∞ accounts for the higher-lying electronic excitations. The phenomenological damping parameters $\Gamma_j>0$ represent finite lifetimes of the excited eigenmodes; they are determined by the energy- and pseudomomentum-conserving transitions to the continuum of multiphonon states. On the other hand, the dielectric polarization due to multiphonon processes is neglected in the above dielectric function. For $\sigma_j=0$, $j=1,\ldots,K$, Eq. (2) describes the response of independent classical oscillators obeying the equations of motion

$$d^2x_j/dt^2+\gamma_j dx_j/dt+\omega_j^2 x_j=e_jE(t), \quad j=1,\ldots,K, \tag{3}$$

where e_j is the effective charge of the jth oscillator.[20] The amplitude x_{0j} of the displacement $x_j(t)=x_{0j}(\omega)\exp(-i\omega t)$ is proportional to the field amplitude E_0 and the effective charge e_j. Consequently, the strengths S_j are proportional to the squares of the effective charges, since the contribution of

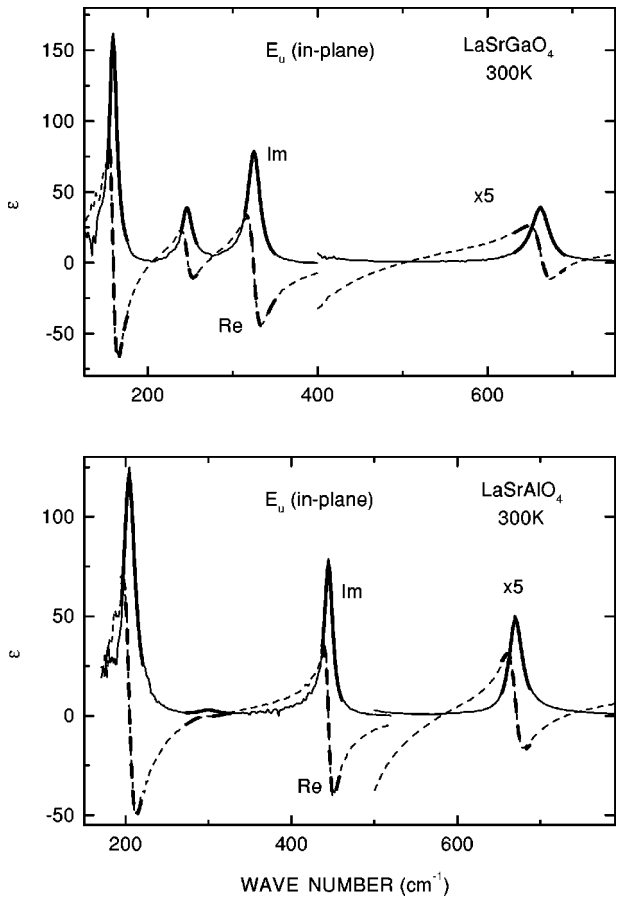

FIG. 5. Same as Fig. 3 for the in-plane components of the dielectric tensor.

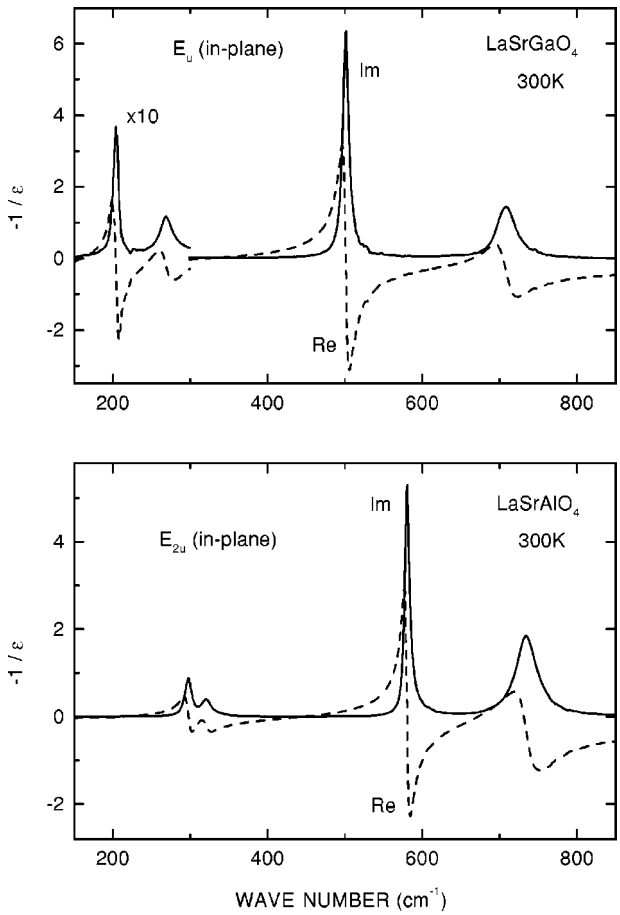

FIG. 6. Same as Fig. 4 for the in-plane components of the dielectric tensor.

the jth mode to the induced dipole moment is proportional to $e_j x_{0j}$. Adding up the dipole moments of these modes, we obtain the dielectric function of Eq. (2) with $\Omega_j=\omega_j$, $\Gamma_j=\gamma_j$, and $\sigma_j=0$ for any j.

The generalization included in Eq. (2), with nonzero real values of σ_j (having dimensions of frequency), is used to describe the response of the system with coupled modes. Since ε has to decrease faster than $1/\omega$ for $|\omega|\to\infty$, the sum of these additional parameters has to vanish,

$$\sum_{j=1}^{K}\sigma_j=0. \tag{4}$$

Equation (4) requires the existence of at least two coupled modes if σ_j are to be finite. In the following equations of motion, the damping forces include contributions proportional to the *relative velocities* of the oscillators:

$$d^2x_j/dt^2+\gamma_j dx_j/dt+\sum_{k=1}^{K}\gamma_{jk}d(x_k-x_j)/dt+\omega_j^2x_j$$
$$=e_jE(t),\quad j=1,\ldots,K. \tag{5}$$

The coupling constants γ_{jk} describe phenomenologically the possible transfer of energy between displacements belonging to the normal modes described by Eq. (3). In our case, the microscopic origin of the coupling of the idealized modes of a hypothetical crystal with identical atoms at the sites of Sr and La is presumably just their stochastic distribution. The redistribution of oscillator strength due to the mode interaction has been discussed in Ref. 20, where its influence on the line shapes of reflectance spectra has been identified.

In order to avoid cumbersome algebra we examine the link between Eqs. (2) and (5) in the case of two coupled modes. This can be done easily if both the broadening γ_1 and γ_2 and the coupling parameters $\gamma_{12}=\gamma_{21}$ are small compared with the resonance frequencies related to the restoring forces ω_1 and ω_2. The algebraic equations for the displacement amplitudes resulting from Eqs. (5) then read

$$(\omega_1^2-\omega^2-i\omega\gamma_1)x_{01}-i\omega\gamma_{12}(x_{01}-x_{02})=e_1E_0,$$
$$(\omega_2^2-\omega^2-i\omega\gamma_2)x_{02}-i\omega\gamma_{12}(x_{02}-x_{01})=e_2E_0. \tag{6}$$

Let us further assume that the separation of the two resonance frequencies is large compared to the broadening and coupling constants. In a narrow frequency range close to ω_1, approximate solutions of Eqs. (6) can be approximated by

$$x_{01}\approx\frac{e_1-i\omega\gamma_{12}e_2/(\omega_2^2-\omega_1^2)}{\omega_1^2+\omega_1^2\gamma_{12}^2/(\omega_2^2-\omega_1^2)-\omega^2-i\omega(\gamma_1+\gamma_{12})}E_0,$$
$$x_{02}\approx\frac{-i\omega\gamma_{12}e_1/(\omega_2^2-\omega_1^2)}{\omega_1^2+\omega_1^2\gamma_{12}^2/(\omega_2^2-\omega_1^2)-\omega^2-i\omega(\gamma_1+\gamma_{12})}E_0. \tag{7}$$

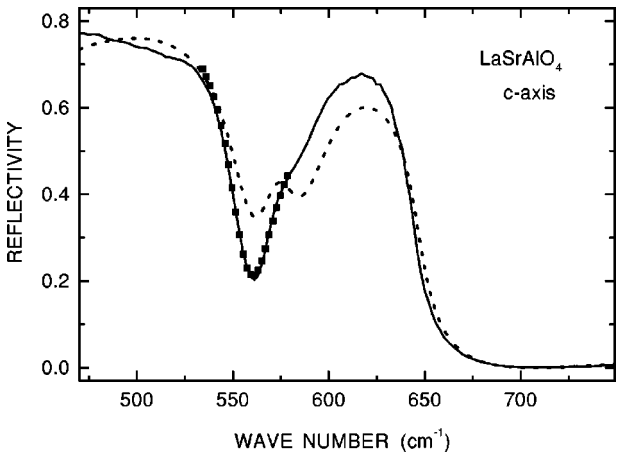

FIG. 7. Room-temperature near-normal incidence reflectivity of $LaSrAlO_4$ polarized along the c axis in the range of the highest TO and LO modes. Solid line: our direct measurement at 10° off normal incidence; dashed line: reflectivity computed from the dielectric function of Ref. 7; symbols: reflectivity computed from the modified Lorentzian parameters of the 568-cm^{-1} mode. Note that the structure at ~580 cm^{-1}, much stronger in the dashed spectrum, is spurious. It is due to the strong and narrow in-plane LO band of $LaSrAlO_4$ at this photon energy.

Thus we have obtained an approximate result for $(e_1x_{01}+e_2x_{02})/E_0$ giving the line shape of ε close to ω_1. It is of the form of the $j=1$ term in the sum of Eq. (2) with

$$\Omega_1=\sqrt{\omega_1^2+\omega_1^2\gamma_{12}^2/(\omega_2^2-\omega_1^2)},\quad \Gamma_1=\gamma_1+\gamma_{12},$$

$$S_1=e_1^2/\Omega_1^2,\quad \sigma_1=2\gamma_{12}e_1e_2/(\omega_2^2-\omega_1^2). \tag{8}$$

Interchange of the subscripts 1 and 2 gives the corresponding approximate line shape in the vicinity of the second resonance frequency ω_2. As expected, the vanishing of the coupling constant γ_{12} implies vanishing of σ_1 and σ_2. The coupling shifts the resonance frequencies independently of the sign of γ_{12}, a fact which reproduces the results of standard second-order perturbation theory. On the other hand, the changes of the linewidths depend on the sign of the coupling constant. Close to the resonances, they appear as a pronounced asymmetry of the line shapes, which results from the mixing of the real and imaginary parts of the spectral profiles of independent modes due to the $-i\omega\sigma_j$ terms in Eq. (2). Note that σ_2 has the same magnitude but opposite sign as σ_1 in Eq. (8). The requirement of Eq. (4) is therefore fulfilled automatically; it is a consequence of the structure of equations of motion. Further, the type of asymmetry of the line shapes depends on the signs of the effective charges and coupling constant, and differs for the two interacting modes due to the changing sign of the difference of their squared frequencies.

In a rough picture, the coupling of a given lattice vibration with more than one of the remaining modes consists in an additive influence on its position, width, and intermixing of the real and imaginary parts of its line shapes. As seen from Eq. (8), the coupling constants determining these changes are weighted by the mode strengths (related to effective charges) and spectral positions. In this work, we restrict the use of the representation of Eq. (2) to narrow intervals close to the mode centers. This enables us to avoid possible problems with unphysical behavior consisting in negative values of the absorptive part ε_2 that can occur for some combinations of parameters on the positive real axis of ω. The dissipative nature of the response function of Eq. (2) for all frequencies can be tested fairly simply for $K=2$.[20] However, it is a difficult task for a larger number of modes.

The asymmetric line shapes of Eq. (2) are similar to the Fano profiles resulting from the quantum interference of a discrete state with a continuum.[21] This is most easily seen for weakly asymmetric profiles [$\sigma_j/\Omega_j \ll 1$ in Eq. (2)]. In fact, introducing the reduced frequency $\epsilon=(\Omega_j-\omega)/(\Gamma/2)$, we can approximate the imaginary part of the j term in the range close to the resonance frequency ω_j by

$$\varepsilon_2 \approx \text{const}-\frac{\sigma_j}{\Gamma_j}\frac{\epsilon-\Omega_j/\sigma_j}{\epsilon^2+1}. \tag{9}$$

This is of the form of the usual Fano line shape, $(\epsilon+q)^2/(\epsilon^2+1)$, in the limit of weak coupling, $q \gg 1$, with $q=-2\Omega_j/\sigma_j$.

We close this subsection with a comment on the so-called factorized form of the dielectric function,

$$\varepsilon(\omega)=\varepsilon_\infty\prod_{j=1}^{K}\frac{\Omega_{\mathrm{LO}j}^2-\omega^2-i\omega\Gamma_{\mathrm{LO}j}}{\Omega_{\mathrm{TO}j}^2-\omega^2-i\omega\Gamma_{\mathrm{TO}j}}, \tag{10}$$

which was introduced in Ref. 22. Here $\Omega_{\mathrm{TO}j}$ and $\Omega_{\mathrm{LO}j}$ denote the frequencies of transverse and longitudinal modes, and $\Gamma_{\mathrm{TO}j}$ and $\Gamma_{\mathrm{LO}j}$ their dampings. It displays readily K pairs of poles in both ε and $-1/\varepsilon$ that are located in the lower half plane of complex ω if all damping parameters are positive. The number of parameters of Eqs. (10) and (2) is the same, and the two forms are essentially equivalent. In fact, ε of Eq. (2) can be expressed as a fraction of two polynomials of degree $2K$, both becoming complex conjugate upon changing the sign of ω. The numerator can then be factorized in the same way as in Eq. (10). When the factorized form is used with no constraints on the TO and LO frequencies and dampings, the function may fail to be dissipative for all frequencies, and also contain a term proportional to $1/\omega$ for $|\omega|\to\infty$. The condition for avoiding the latter deficiency should be equivalent to Eq. (4). It can be found from the following requirement: $d\varepsilon(\xi)/d\xi|_{\xi=0}=0$, $\xi=1/\omega$. After a simple differentiation in Eq. (10) we arrive at

$$\sum_{j=1}^{K}\Gamma_{\mathrm{TO}j}=\sum_{j=1}^{K}\Gamma_{\mathrm{LO}j}. \tag{11}$$

Let us note that the independent oscillators give ε vanishing as $1/\omega^2$ for $|\omega|\to\infty$. They therefore fulfill Eq. (4) [which is trivial when all σ_j in Eq. (2) vanish] and also Eq. (11). Although the dampings of independent TO and LO modes, except for $K=1$, may differ, their sums should be equal; however, overlaping broad bands of multiphonon or impurity absorption can influence significantly the situation in the LO range.[15] We prefer here the model line shapes in the form of Eq. (2) because of the relationships provided by Eqs. (8). The factorized form has also been used in recent reflectivity studies of LSGO and LSAO,[7] and we discuss the parametrization below.

TABLE II. Mode parameters obtained from the fit of modified Lorenztians to ε (TO modes) and to $-1/\varepsilon$ (LO modes). The strength S is dimensionless, all other parameters are in cm^{-1}. The rows denoted by (a) list phonon energies and broadenings obtained from reflectivity measurements; note that the number of reported modes is larger than required by symmetry and observed in our work, except for the E_u modes of $SrLaGaO_4$. The rows denoted by (b) list the phonon energies estimated for $LaSrAlO_4$ from reflectivity spectra and calculated using a shell model.

$LaSrGaO_4$ mode	S_{TO}	σ_{TO}	Ω_{TO}	Γ_{TO}	Ω_{LO}	Γ_{LO}	Ref.
			A_{2u} (c axis)				
1	1.2	46	138	16	140	18	
			139	17	142	20	7
2	16.3	−60	254	61	514	24	
			258	69	498	27	7
3	0.05	11	525	20	597	39	
			522	23	518	16	7
			510	46	600	35	7
			E_u(in-plane)				
1	11.4	−66	159	11	204	8	
			162	13	204	9	7
2	2.2	108	246	15	263	33	
			246	16	270	24	7
3	4.2	−64	326	18	501	9	
			328	22	502	9	7
4	0.3	7	663	26	709	28	
			658	27	707	25	7
$LaSrAlO_4$							
			A_{2u} (c axis)				
1	9.0	−31	251	19	323	61	
			246	26	309	60	7
			234		364		6, expt
			272		315		6, calc
2	1.2	13	343	38	555	23	
			348	80	426	110	7
			444	100	558	27	7
			379		430		6, expt
			384		510		6, calc
3	0.078	17	568	24	643	13	
			567	22	580	26	7
			589	33	646	13	7
			610		620		6, expt
			597		635		6, calc
			E_u(in-plane)				
1	10.1	94	204	17	297	11	
			208	12	298	8	7
			204		393		6, expt
			222		255		6, calc
2	0.2	47	299	18	320	15	
			313.1	11	312.6	13	7
			314		316		6, expt
			314		316		6, calc
3	2.1	−130	445	13	580	7.5	
			447	6	582	6	7
			460		582		6, expt
			422		502		6, calc
4	0.3	5	670	20	734	32	
			668	22	707	48	7
			713	40	735	38	7
			666		687		6, expt
			663		759		6, calc

C. TO and LO modes of $LaSrGaO_4$ and $LaSrAlO_4$

We have fitted the strongest bands in the spectra of the room-temperature dielectric function and its negative inverse of Figs. 3–6 with the asymmetric line shapes of Eq. (2); the best-fit line shapes are shown in the fitted segments of the spectra of ε by thick lines. Resulting fit parameters are listed in Table II. The $-1/\varepsilon$ spectra were found to be fitted fairly well with uncoupled modes, i.e., using all σ_j in Eq. (2) fixed at zero. We restrict therefore the results for LO modes to their positions and widths.

In Table II we also list data found in the literature. They are generally in fair agreement with our results, except for the occurrence of additional modes in Ref. 7, as discussed above. The positions computed[6] using a shell model for $LaSrAlO_4$ are reasonably close to the observed ones, except for the 580 cm^{-1} in-plane LO mode. It should be noted that the parametrization of Ref. 7 produces negative values of ε_2 at high frequencies for both LSGO and LSAO. We reemphasize, however, that our representation does not pretend to be accurate for all frequencies; instead, it is intended to extract properties of the strongest vibrational modes. In any case, the requirements of Eqs. (4) and (11) are reasonably well fulfilled by the parameters in Table II resulting from our study, with the experimental uncertainty of the broadenings being below $\sim 5\%$. The same is true for the reflectivity data[7] after a correction for the extra modes.

We have tested the reliability of the determination of the asymmetry parameters σ_j that are related to the mode coupling. In Fig. 8 we show the room- and low-temperature data of the 326 cm^{-1} in-plane mode of LSGO which has the width of 18 cm^{-1} at 300 K. The broadening parameter is reduced to 11 cm^{-1} at 10 K, while the resulting strength, $S = 4.1$, remains almost unchanged. The value of σ at 10 K is -73 cm^{-1}, close to the room-temperature result of -64 cm^{-1}; a difference of about 10 cm^{-1} is within our experimental uncertainties in this case. Consequently, the interaction of this mode with the remaining ones can be assumed to be temperature independent, as expected for the coupling mediated by disorder. Note that the negative sign of σ means the flatter rise and steeper fall of the absorption when going

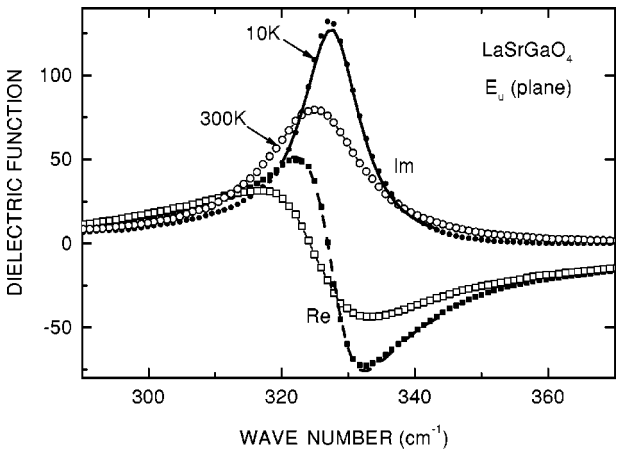

FIG. 8. The in-plane spectra of the 326-cm^{-1} mode of $LaSrGaO_4$ at 300 K (open symbols) and 10 K (solid symbols). The best-fit modified Lorentzians (solid and dashed lines) reproduce well the band asymmetry, showing no change of the mode strength and coupling parameter with changing temperature.

across the band from lower to higher energies seen in Fig. 8. This level of asymmetry is easily detectable: the ratio of imaginary and real parts of the numerator in Eq. (2) at the mode center is $\sigma/(S\omega)\approx -0.05$.

The 568 cm^{-1} c-axis mode of LSAO displays an opposite type of asymmetry manifesting itself in the positive sign of

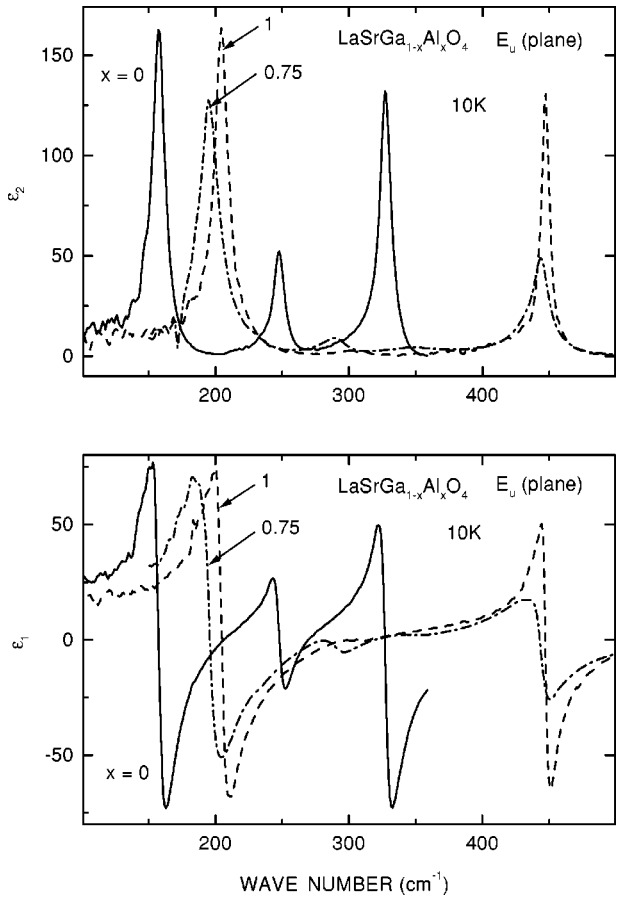

FIG. 9. The real (lower panel) and imaginary (upper panel) parts of the in-plane component of the dielectric tensor of $LaSrGaO_4$ (solid lines), $LaSrAlO_4$ (dashed lines), and $LaSrGa_{0.25}Al_{0.75}O_4$ (dash-dotted lines) crystals, at 10 K.

TABLE III. Zone-center phonon frequencies in cm^{-1} of several T-structure materials.

	TO modes				
Compound	$A_{2u}(1)$	$A_{2u}(2)$	$A_{2u}(3)$		Ref.
$LaSrAlO_4$	568	343	251		this work
$LaSrGaO_4$	525	254	138		this work
La_2NiO_4	490	347	220		2, neutrons
	503	275			27, IR reflectance
	515	370	280		1, IR reflectance
La_2CuO_4	495	250	150		28, neutrons
	500	235	135		3, IR ellipsometry
	501	342	242		29, IR reflectance
	$E_u(1)$	$E_u(2)$	$E_u(3)$	$E_u(4)$	
$LaSrAlO_4$	670	445	299	204	this work
$LaSrGaO_4$	663	326	246	159	this work
La_2NiO_4	650	350	220	150	2, neutrons
	656	351	224	151	27,IR reflectance
	675	367	236	150	1, IR reflectance
La_2CuO_4	680	350	170	120	28, neutrons
	667	358		132	29, IR reflectance
	695	360		145	1, IR reflectance
	LO modes				
	$A_{2u}(1)$	$A_{2u}(2)$	$A_{2u}(3)$		
$LaSrAlO_4$	643	555	323		this work
$LaSrGaO_4$	597	514	140		this work
La_2NiO_4		440			2, neutrons
	574	472			27, IR reflectance
La_2CuO_4	575	458			30, IR reflectance
	$E_u(1)$	$E_u(2)$	$E_u(3)$	$E_u(4)$	
$LaSrAlO_4$	734	580	320	297	this work
$LaSrGaO_4$	709	501	263	204	this work
La_2NiO_4	665	391	243	171	27, IR reflectance
La_2CuO_4	685	450	280	165	28, neutrons

σ. Its contribution to the absorption falls steeply when going across the band to lower energies; this is accompanied by a steep rise of the near-normal reflectance shown in Fig. 7, which cannot be reproduced by an independent oscillator with a high value of its broadening parameter required by the spectral form of the dip in reflectivity. Here, the situation is similar to the case of perovskites studied in Ref. 20. The corresponding mode of LSGO has similar coupling to the two lower bands. However, unlike the case of the perovskites, none of the three c-axis modes seems to be uncoupled from the others. The weakest coupling, on the verge of being observable, occurs for the high-frequency in-plane vibrations of both LSGO and LSAO.

A pronounced contribution to the mode coupling can be expected in $SrLaGa_{1-x}Al_xO_4$ alloys, with additional randomness in the occupation of the centers of MO_6 octahedra with $M=$Al or Ga atoms. We show in Fig. 9 the low-temperature in-plane spectra of both constituents and the $x=0.75$ mixed crystal. Note that the 445-cm^{-1} mode of

LSAO (having the highest coupling parameter) moves much less towards lower energies with adding Ga than the two lower bands. At the same time, its asymmetry increases. A possible explanation consists in an upward repulsion due to the increased interaction with remaining modes at this high level of coupling. It should also be noted that the weak band centered at $\sim$300 cm^{-1} in LSAO becomes much better resolved upon adding Ga.

A comparison of our results with other optical and neutron-scattering studies of several *T*-structure materials is presented in Table III. Together with the results of lattice dynamics calculations that provide displacement patterns of normal modes,[23,2,24,6] it allows us to formulate the following mode assignment for LSGO and LSAO. We will also mention the implications of this assignment for $La_{2-x}Sr_xCuO_4$, with its atomic masses fairly close to LSGO. The square roots of the mass ratios, $\sqrt{(}m_M/m_{Cu}$, are 1.05, 0.96, and 0.65 for $M=$Ga, Ni, and Al, respectively.

A_{2u} modes. The two high-frequency TO modes $A_{2u}(1)$ and $A_{2u}(2)$ correspond essentially to bond stretching and bending, respectively; they were predicted by lattice-dynamical calculations to be at 490 and 347 cm^{-1} in La_2NiO_4, (Ref. 2) and 446 and 197 cm^{-1} in La_2CuO_4.[24] The lowest band calculated at 220 cm^{-1} in La_2NiO_4 (Ref. 2) and 119 cm^{-1} in La_2CuO_4,[24] is characterized by rather small displacements of in-plane oxygens. We believe that the 138-cm^{-1} mode of LSGO is analogous to the weak 135-cm^{-1} band of La_2CuO_4 identified in the IR data of Ref. 3. The data for LO modes are scarce; the only reliably identified LO phonon seems to be the highest, related to the 663-cm^{-1} mode of LSGO.

E_u modes. The highest TO mode $E_u(1)$ (doubly degenerate) corresponds to in-plane bond stretching; its frequencies obtained in various studies are in very good agreement with each other. The remaining three TO phonon frequencies of Table III are fairly close except for the consistently higher values for LSAO. The $E_u(2)$ and (3) modes are primarily bond bending motions of the MO_6 octahedra; as suggested by the eigenvectors computed for La_2NiO_4 (Ref. 2) and La_2CuO_4,[24] they contain significant displacements of the central atoms in both compounds. The ''missing'' phonon of E_u symmetry for La_2CuO_4 (Ref. 1) is likely to be located below the strong mode at $\sim$350–360 cm^{-1} (326 cm^{-1} in LSGO), not at $\sim$400 cm^{-1} as suggested in Ref. 1. Our estimate points to a position not far from that in LSGO (246 cm^{-1}). The lowest mode, $E_u(4)$, is probably the motion of La/Sr ions against the MO_6 octahedra.[2] The eigenvector pattern computed[24] for La_2CuO_4 displays, on the contrary, a very small displacement of the Cu atom, while producing an unstable mode with imaginary frequency. In the experimental spectra, the mode positions are fairly close. The in-plane LO phonons are generally more difficult to measure in conducting materials. Taking this into account, the LO data in Table III for La_2NiO_4, a material with fairly high in-plane conductivity are in reasonable agreement with both LSGO and La_2CuO_4. The good agreement of the positions of $E_u(3)$ LO mode of LSGO, La_2NiO_4, and La_2CuO_4 provides further evidence for an upper limit of the second lowest TO mode of La_2CuO_4. Namely, it should be located below $\sim$280 cm^{-1}, which is the highest of the three entries.

IV. CONCLUSION

We have used ellipsometric and reflectance techniques to study the infrared response of anisotropic crystals of LSGO and LSAO. We have observed the proper number of infrared-active phonons required by crystal symmetry. An extremely high optical contrast between the ordinary and extraordinary response in the range of sharp LO modes is found to require special care to avoid spurious spectral structures. The lattice bands of LSGO and LSAO show pronounced features of mode coupling, due to the random distribution of La and Sr atoms in the lattice. We have presented a scheme to identify and quantify the coupling. Some of the features found here are similar to those observed in anharmonic perovskites.[20] The positions of transverse and longitudinal phonon modes of LSGO are found to be useful in discussing the vibrational properties of other interesting compounds crystallizing in the same or similar structure. In particular, our results confirm the proposed assignment of the *c*-polarized vibrations[3] and predict the frequency of the missing weak in-plane phonon of La_2CuO_4.

ACKNOWLEDGMENTS

One of us (J.H.) acknowledges the hospitality of the Max-Planck-Institut für Festkörperforschung Stuttgart. We are indebted to M. Berkowski for providing the samples, to D. Munzar and C. Bernhard for helpful discussions, and to D. Böhme and R. Švehla for technical help.

*Permanent address: Department of Solid State Physics, Faculty of Science, Masaryk University, Kotlářská 2, 611 37 Brno, Czech Republic.

[1] S. Tajima, T. Ido, S. Ishibashi, T. Itoh, H. Eisaki, Y. Mizuo, T. Arima, H. Takagi, and S. Uchida, Phys. Rev. B **43**, 10 496 (1991).

[2] L. Pintschovius, J. M. Bassat, P. Odier, F. Gervais, G. Chevrier, W. Reichardt, and F. Gompf, Phys. Rev. B **40**, 2229 (1989).

[3] R. Henn, A. Wittlin, M. Cardona, and S. Uchida, Phys. Rev. B **56**, 6295 (1997).

[4] R. Brown, V. Pendrick, D. Kalokitis, and B. H. T. Chai, Appl. Phys. Lett. **57**, 1351 (1990).

[5] C. Le Paven-Thivet, M. Guilloux-Viry, J. Padiou, A. Perrin, M. Sergent, L. A. de Vaulchier, and N. Bontemps, Physica C **244**, 231 (1995).

[6] V. G. Hadjiev, M. Cardona, I. Ivanov, V. Popov, M. Gyulmezov, M. N. Iliev, and M. Berkowski, J. Alloys Compd. **251**, 7 (1997).

[7] S. Kamba, E. Buixaderas, and A. Pajaczkowska, Phys. Status Solidi A **168**, 317 (1998).

[8] R. D. Shannon, R. A. Oswald, J. B. Parise, B. H. T. Chai, B. Byszewski, A. Pajaczkowska, and R. Sobolewski, J. Solid State Chem. **98**, 90 (1992).

[9] A. Gloubokov, R. Jablonski, W. Ryba-Romanowski, J. Sass, A. Pajaczkowska, R. Uecker, and P. Reiche, J. Cryst. Growth **147**, 123 (1995).

[10] W. Ryba-Romanowski, S. Golab, I. Sokólska, W. A. Pisarski, G.

Dominiak-Dzik, A. Pajaczkowska, and M. Berkowski, J. Alloys Compd. **217**, 263 (1995).
[11] J. Hora, K. Navrátil, J. Humlíček, and M. Berkowski, Phys. Status Solidi B **195**, 625 (1996).
[12] R. Henn, Ph.D. thesis, MPI Stuttgart, 1997.
[13] J. Humlíček, Ferroelectrics **176**, 221 (1996).
[14] R. M. A. Azzam and N. M. Bashara, *Ellipsometry and Polarized Light* (North-Holland, Amsterdam, 1977).
[15] J. Humlíček, Philos. Mag. B **70**, 699 (1994).
[16] J. Humlíček and K. Vojtěchovský, Phys. Status Solidi A **92**, 249 (1985).
[17] D. E. Aspnes, J. Opt. Soc. Am. **70**, 1275 (1980).
[18] J. Humlíček, Thin Solid Films **313-314**, 687 (1998).
[19] D. L. Rousseau, R. P. Bauman, and S. P. S. Porto, J. Raman Spectrosc. **10**, 253 (1981).
[20] A. S. Barker, Jr. and J. J. Hopfield, Phys. Rev. **135**, A1732 (1964).
[21] U. Fano, Phys. Rev. **124**, 1866 (1961).
[22] D. W. Berreman and F. C. Unterwald, Phys. Rev. **174**, 791 (1968).
[23] R. E. Cohen, W. E. Pickett, H. Krakauer, and L. L. Boyer, Physica B **150**, 61 (1988).
[24] D. J. Singh, Solid State Commun. **98**, 575 (1996).
[25] M. Drozdowski, J. Domagala, M. Kozielski, M. Szybowicz, and A. Pajaczkowska, Solid State Commun. **98**, 785 (1995).
[26] M. Berkowski (private communication).
[27] F. Gervais, P. Echegut, J. M. Bassat, and P. Odier, Phys. Rev. B **37**, 9364 (1988).
[28] L. Pintschovius, N. Pyka, W. Reichardt, A. Yu. Rumiantsev, N. L. Mitrofanov, A. S. Ivanov, G. Collin, and P. Bourges, Physica C **185-189**, 156 (1991).
[29] R. T. Collins, Z. Schlesinger, G. V. Chandrasekhar, and M. V. Shafer, Phys. Rev. B **39**, 2251 (1989).
[30] M. A. Quijada, D. B. Tanner, F. C. Chou, D. C. Johnston, and S.-W. Cheong, Phys. Rev. B **52**, 15 485 (1995).